 Preprint from Nuclear Instruments and Methods in Physics Research B 371 (2016) 59–62

Drawing the geometry of 3d transition metal-boron pairs in silicon from electron emission channeling experiments

D.J. Silva [a], *, U. Wahl [b], J.G. Correia [b], V. Augustyns [a], T.A.L. Lima [a], A. Costa [b], E. Bosne [b], M.R. da Silva [c], J.P. Araújo [d], L.M.C. Pereira [a]

[a] *KU Leuven, Instituut voor Kern- en Stralingsfysica, 3001 Leuven, Belgium*
[b] *Centro de Ciências e Tecnologias Nucleares, Instituto Superior Técnico, Universidade de Lisboa, 2695-066 Bobadela, Portugal*
[c] *Centro de Física Nuclear da Universidade de Lisboa, 1649-003 Lisboa, Portugal*
[d] *IFIMUP and IN-Institute of Nanoscience and Nanotechnology, Departamento de Física e Astronomia da Faculdade de Ciências da Universidade do Porto, 4169-007 Porto, Portugal*

* Corresponding author, email: djsilva99@gmail.com

DOI: http://dx.doi.org/10.1016/j.nimb.2015.09.051

Abstract

Although the formation of transition metal-boron pairs is currently well established in silicon processing, the geometry of these complexes is still not completely understood. We investigated the lattice location of the transition metals manganese, iron, cobalt and nickel in *n*- and p^+-type silicon by means of electron emission channeling. For manganese, iron and cobalt, we observed an increase of sites near the ideal tetrahedral interstitial position by changing the doping from *n*- to p^+-type Si. Such increase was not observed for Ni. We ascribe this increase to the formation of pairs with boron, driven by Coulomb interactions, since the majority of iron, manganese and cobalt is positively charged in p^+-type silicon while Ni is neutral. We propose that breathing mode relaxation around the boron ion within the pair causes the observed displacement from the ideal tetrahedral interstitial site. We discuss the application of the emission channeling technique in this system and, in particular, how it provides insight on the geometry of such pairs.

1. Introduction

To mitigate the detrimental electrical effects of transition metals (TMs) in silicon, several approaches, commonly known as gettering techniques, have been developed to remove the TMs from the active regions of the devices [1]. One well known approach consists of using *p*-type layers rich in immobile boron dopants which bind positively charged TM impurities via Coulomb interaction. In fact, most of the TMs introduce deep donor levels in the lower region of the silicon bandgap, which results in changes in their charge states. For instance, Fe is known to introduce a deep donor level close to the valence band, hence being most likely positively charged in *p*-type silicon. Therefore, Fe can easily interact with B^-. Previous studies based on Mössbauer spectroscopy (MS) and electron paramagnetic resonance (EPR), which are sensitive to the local environment of the TMs, addressed the configuration of such pairs [1–5]. The results showed that the local environment of Fe has a trigonal <111> symmetry, within FeB pairs [6–8]. This symmetry may correspond to the closest tetrahedral interstitial site of the substitutional B^-. Density functional theory calculations have also predicted a similar structure, however with a breathing mode relaxation around the B^- ion [9]. One way to gain deeper insight into the configuration of these defect complexes is by determining the exact location of the transition metal in the lattice. In that respect, electron emission channeling is currently the most suited technique to obtain such information, where the location of radioactive isotopes is deduced from the channeling effects of the β^- particles emitted by probe atoms. We note that in comparison to ion beam lattice location techniques of implanted impurities, e.g. by means of backscattering, emission channeling has four orders of magnitude higher efficiency, which allows performing detailed lattice location investigations of impurities at low concentrations [10]. In this work, we determined experimentally the lattice location of the implanted 3*d* TMs ^{56}Mn, ^{59}Fe [11], ^{61}Co [12] and ^{65}Ni [13] in *n*- and p^+-type silicon by means of electron emission channeling.

2. Experiment

The emission channeling (EC) technique is based on the observation of channeling effects along some crystallographic directions, which depends on the location of the emitters. The observed electron yield with respect to the main crystallographic directions is fitted to theoretical patterns obtained with the *manybeam* formalism [14]. Such approach can distinguish positions separated by as little as ~0.03 Å. EC investigations have been performed at the ISOLDE facility at CERN [15,16], where radioactive isotopes are produced via spallation, fission or fragmentation reactions in thick targets, induced by proton beams from a proton synchrotron booster (PSB) at energies and intensities to up to 1.4 GeV and 2 μA, respectively. The volatile nuclear reaction products are then released from the high temperature target. In order to ionize the desired chemical element, a resonance ionization laser ion source is used [17]. Radioactive isotope ions are then accelerated up to 60 keV. This unique process is coupled to powerful mass separators from which radioactive beams of high isotopic purity are produced. In this work we used ^{56}Mn ($t_{1/2}$ = 2.57 h) and ^{65}Ni ($t_{1/2}$ = 2.5 h) probes, which were directly obtained as radioactive ion beams, and ^{59}Fe and ^{61}Co probes obtained by implanting the precursor isotopes ^{59}Mn ($t_{1/2}$ = 4.6 s) and ^{61}Mn ($t_{1/2}$ = 0.61 s), respectively. ^{61}Co followed the decay chain ^{61}Mn → ^{61}Fe (5.98 min) → ^{61}Co, while ^{59}Mn is already the parent of ^{59}Fe. Note that both ^{59}Fe and ^{61}Co are recoiled with sufficient energies (200 eV and 103 eV respectively) to erase the implantation history of the parent isotopes. The details of each experiment, which include the properties of the different Si samples and the implantation conditions, are shown in Table 1. Each electron emission channeling experiment consisted generally of: ion implanting the radioactive isotope, performing an isochronal annealing treatment for 10 min, and orienting the sample and further measuring the electron yield in the vicinity of several crystallographic directions at room temperature. While ^{59}Fe was ion implanted and measured in separate chambers, ^{56}Mn, ^{61}Co and ^{65}Ni were implanted and measured inside the same chamber at the end of one of the beamlines of the ISOLDE facility, i.e. online.

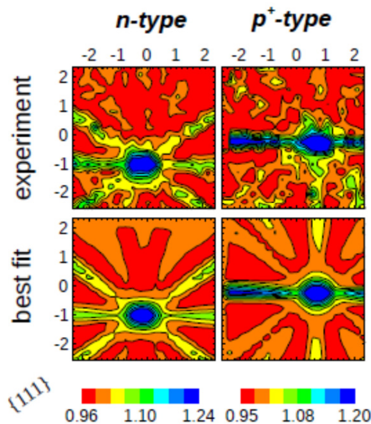

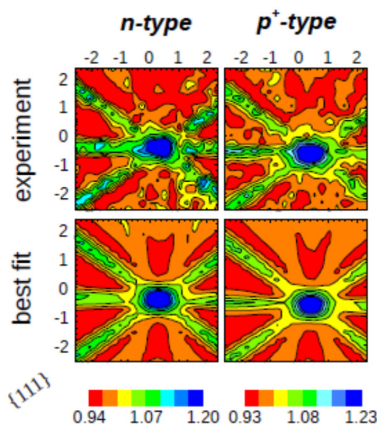

Fig. 1. Two dimensional experimental patterns and corresponding best fits from (a) ^{61}Co and (b) ^{65}Ni, in the vicinity of <110> following ion implantation at room temperature, for n-type and p^+-type silicon samples.

3. Results

The two-dimensional experimental patterns were fitted by theoretical β^- emission yields for emitters, calculated with the *manybeam* formalism for electron channeling [14]. A range of lattice sites were considered in the theoretical patterns covering the following relevant high symmetry sites: substitutional (S), hexagonal (H), tetrahedral (T), bond-centered (BC), anti-bonding (AB), split (SP) and the so-called DS, DT, Y and C sites. Sites displaced from these high symmetry sites along <111>, <100> and <110> were also considered. The minimum step of displacement was ~0.03 Å. These lattice sites are discussed in detail in Ref. [13]. The minimization of the χ^2 of fit resulted consistently in the identification of three lattice sites: ideal substitutional sites (S sites), sites displaced from BC towards S sites (near-BC sites), and sites displaced from T towards AB sites (near-T sites). The experimental patterns in the vicinity of <110> and best fit patterns following ion implantation at room temperature for ^{61}Co and ^{65}Ni, as well as the dependence of the near-T fraction on the annealing temperature for all the four TMs are plotted in Figs. 1 and 2(a), respectively. The energy level scheme of each TM is also represented in Fig. 2(b). For Mn, Fe and Co, the change of doping from n- to p^+-type Si reduced channeling effects along {111} and {311} planes. One example can be seen in Fig. 1(a) where channeling effects along {111} planes drop from *n*- to p^+-type Si. These blocking effects are characteristic of lattice sites near the ideal T position. On the contrary, no change was observed for Ni (see Fig. 1(b) for the as-implanted state). In p^+-type silicon, the displacement from the ideal T site ranges from 0.00 to 0.81 Å for Mn, Co and Fe, and from 0.1 to 1.43 Å for Ni.

Table 1.
Sample and implantation details of the 8 experiments analyzed in the present work.

Transition metal	Silicon material	Resistivity (Ω cm)	Dopant concentration (cm^{-3})	Implantation energy (keV)	Fluence (cm^{-2})	[TM] peak (cm^{-3})
Mn	*n*-Si:P	3–12	$\sim 2 \times 10^{15}$	30	2.4×10^{13}	7.2×10^{18}
	p^+-Si:B	$(4.6–5.9) \times 10^{-3}$	$\sim 3 \times 10^{19}$	30	3.6×10^{13}	1.1×10^{19}
Fe	*n*-Si:P	7.8–12	$\sim 2 \times 10^{15}$	60	6.0×10^{12}	1.1×10^{18}
	p^+-Si:B	< 0.002	$> 6 \times 10^{19}$	60	6.0×10^{12}	1.1×10^{19}
Co	*n*-Si:P	7.8–12	$\sim 2 \times 10^{15}$	50	1.5×10^{12}	3.8×10^{17}
	p^+-Si:B	$(4.6–5.9) \times 10^{-3}$	$\sim 3 \times 10^{19}$	50	1.4×10^{12}	3.8×10^{17}
Ni	*n*-Si:P	7.8–12	$\sim 2 \times 10^{15}$	50	2.4×10^{13}	5.0×10^{18}
	p^+-Si:B	$(1–5) \times 10^{3}$	$\sim 6 \times 10^{19}$	50	3.2×10^{13}	6.0×10^{18}

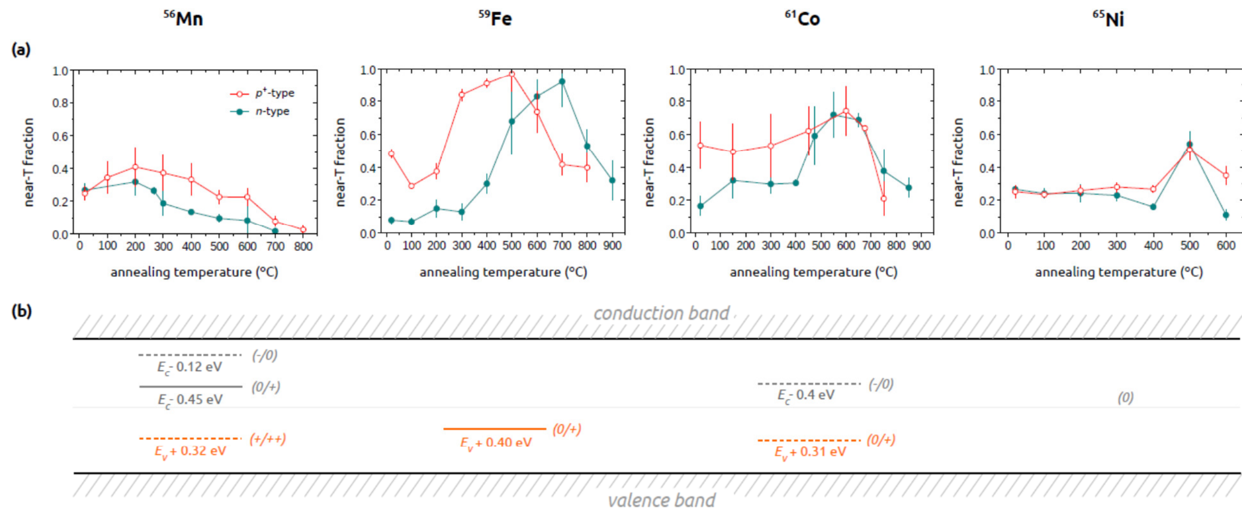

Fig. 2. (a) Dependence of the near-T fraction on the annealing temperature for ^{56}Mn, ^{59}Fe and ^{61}Co and ^{65}Ni in *n*- and p^+-type Si. (b) Energy level diagram for each TM when in their interstitial state. The dashed lines represent levels that are still controversial, while continuous lines represent energy levels well accepted. The orange lines regards the deep donor levels that has some implications on the charge state when changing the doping from *n*- to p^+-type Si [3,5,6,18,19]. (For interpretation of the references to color in this figure legend, the reader is referred to the web version of this article.)

4. Discussion

Because all identified lattice sites are observed in different doping types, one can conclude that they are at least partially associated with vacancies, including the p^+-type Si case. Indeed, from previous investigations [11–13], we suggested that when forming complexes with vacancy-related defects, 3*d* TMs tend to occupy ideal S sites, most likely resulting from the trapping into single vacancies, and near-BC sites and near-T sites, most likely resulting from the trapping into multivacancies. However, the fact that the near-T fraction increases with the doping from *n*- to p^+-type Si shows that additional point defects are involved, namely dopants. In fact, it is well known that the implantation defects anneal with increasing temperature, attaining the full recovery of the crystal at approximately 400 °C. Once the TMs dissociate from the multivacancy complexes, they will diffuse fast and the probability of formation of TM dopant pairs will increase drastically. This may explain the larger near-T fraction observed in p^+-type Si of Fe, Co and Mn compared to *n*-type Si. From the energy level scheme of Fig. 2(b), it is clear that only Ni interstitial impurities do not change their charge state when the Fermi level shifts from the midgap (intrinsic silicon) to a position closer to the valence band (p^+-type Si), due to the absence of any deep energy level within the silicon bandgap. For the case of the other investigated TMs, the charge state changes from 0 to +1 or from +1 to +2. This of course depends on the level of doping. However, when using highly doped p^+-type Si, such charge state change is still favored, as long as the *p*-type doping is high enough to avoid being fully compensated by implantation induced defects. Therefore, the majority of Mn, Co and Fe is positively charged in p^+-type Si, while Ni is neutral irrespective of the doping type. This fact can be easily correlated with the blocking effects mentioned above, corresponding to an increase of the near-T fraction from *n*- to p^+-type Si for Mn, Fe and Co. In fact, it is known that positive interstitial Mn, Co and Fe easily pair with B^-, since the mechanism of pairing is mainly ruled by the Coulomb interaction [1–6], including implanted samples [8]. Such a mechanism avoids Ni to combine with B^- in detectable quantities. Part of the near-T sites of Mn, Fe and Co thus corresponds to TMs which are bound in such pairs. Note that the formation of TM-multivacancy complexes is mostly driven by the lattice potential caused by open volumes or strain, and not by Coulomb interactions.

The only available and complete theoretical work on the geometry of TM-B pairs deals with Fe, where ab initio calculations have shown that the most energetically favorable position of Fe is the ideal T site [9]. Evidence of such configuration was given by MS measurements which have shown that the local environment of Mn, Co and Fe has a trigonal <111> symmetry [2,6]. In the present work, we show that the TMs occupy a displaced rather than an ideal T site. In that respect, one should note that the binding energies for such pairs, already obtained experimentally, imply that the distance between the TM and the boron ion is slightly different from 2.35 Å, which may result in some relaxation of the lattice. According to ab initio calculations a breathing mode relaxation is present around the boron atom, with the four Si nearest neighbors displaced by 0.27 Å. Although the Fe atom is located on one of the next ideal T sites, this relaxation is likely to result in a measurable displacement [9]. The displacement of the near-T sites of Fe, Co and Mn reduces from 0.8 Å to 0.6 Å at room temperature when changing the doping from *n*- to p^+-type, which strengthens the notion that a large part of the near-T sites are due to TM-boron pairs.

Three different types of dependence of the near-T fraction with the annealing temperature can be observed (see Fig. 2(b)). The first regards Fe and Co, while the second and third are observed for Mn and Ni, respectively. Fe and Co show a significant increase of the near-T fraction from *n*- to p^+-type silicon already in the asimplanted state. The fact that the near-T fraction increases in both doping types following annealing above 300 °C indicates that the majority of complexes involved in this annealing temperature range is related to the multivacancies formed during the ion implantation, and not with the pairs with boron. Although Mn is positively charged in p^+-type Si, its charge state is also positive in intrinsic (or low doped but highly compensated) silicon (see Fig. 2 (b)). Moreover, Mn was implanted at lower energies, which results in a depth profile located closer to the surface where band-bending and Fermi-level pinning can occur, reducing the effects of doping. These two facts might have resulted in a slightly different behavior of the near-T fraction of Mn when compared to Fe and Co, however with an unambiguous increase of the near-T fraction from *n*- to p^+-type silicon. Finally, the near-T fraction does not change at all from *n*- to p^+-type Si for the case of Ni. Again, the charge state plays an important role in preventing the formation of NiB pairs. Note that in both doping types the near-T fraction of Ni increases with the annealing temperature. Such complexes are similar to the complexes involving Fe and Co in the 400–800 °C annealing temperature range.

In summary, for Fe and Co, our data supports the notion that pairs with boron are easily formed at room temperature and after annealing at low temperatures, while annealing between ~400 °C and ~800 °C results in the formation of multivacancy complexes where the transition metal also occupies near-T sites. After annealing at high temperatures

the dissociation of the transition metals from the multivacancies also stimulate the reformation of boron pairs, although most of them are formed deeper in the sample (i. e. away from the confined region that enables the observation of channeling effects). Mn also forms pairs with boron but shows some differences with respect to the dependence of the near-T fraction on the annealing temperature, i.e. the number of near-T sites is increased with the doping from *n*- to p^+ for all the annealing temperatures, except after implanting at room temperature. The fact that no substantial differences were observed for Ni when changing the doping is consistent with its neutral charge state.

5. Conclusion

We experimentally investigated the lattice location of Mn, Fe and Co when pairing with boron dopants by means of electron emission channeling. We found that a fraction of sites near the ideal tetrahedral interstitial site increases from *n*- to p^+-type silicon for Mn, Fe and Co. On the contrary, the interstitial fraction did not vary at all with the doping type in the case of Ni. These findings support the notion that the charge state of the transition metal plays a decisive role in the pairing mechanism between the transition metals and boron. We propose that breathing mode relaxation around the boron ion within the pair causes the observed displacement from the ideal tetrahedral interstitial site.

Acknowledgments

This work was supported by FCT-Portugal, project CERN-FP-123585–2011, and by the European Union FP7-through ENSAR, contract 262010. Project Norte-070124-FEDER-000070, Fund for Scientific Research-Flanders and the KU Leuven BOF (CREA/14/013 and STRT/14/002) are acknowledged. D.J. Silva is thankful for FCT Grant SFRH/BD/69435/2010.

References

[1] T. Dietl, Nat. Mater. 9 (2010) 965.
[2] L.M.C. Pereira, U. Wahl, S. Decoster, J.G. Correia, M.R. da Silva, A. Vantomme, J.P. Araújo, Appl. Phys. Lett. 98 (2011) 201905.
[3] L.M.C. Pereira, U. Wahl, S. Decoster, J.G. Correia, L.M. Amorim, M.R. da Silva, J.P. Araujo, A. Vantomme, Phys. Rev. B 86 (2012) 125206.
[4] T. Jungwirth, K.Y. Wang, J. Masek, K.W. Edmonds, J. Konig, J. Sinova, M. Polini, N.A. Goncharuk, A.H. MacDonald, M. Sawicki, A.W. Rushforth, R.P. Campion, L.X. Zhao, C.T. Foxon, B.L. Gallagher, Phys. Rev. B 72 (16) (2005) 165204.
[5] T. Shi, S. Zhu, Z. Sun, S. Wei, W. Liu, Appl. Phys. Lett. 90 (2007) 102108.
[6] Z. Sun, W. Yan, G. Zhang, H. Oyanagi, Z. Wu, Q. Liu, W. Wu, T. Shi, Z. Pan, P. Xu, S. Wei, Phys. Rev. B 77 (2008) 245208.
[7] N. Farley, K. Edmonds, A. Freeman, G. van der Laan, C. Staddon, D. Gregory, B. Gallagher, New J. Phys. 10 (2008) 055012.
[8] J.C. Pivin, G. Socol, I. Mihailescu, P. Berthet, F. Singh, M.K. Patel, L. Vincent, Thin Solid Films 517 (2008) 916.
[9] A. Bonanni, M. Sawicki, T. Devillers, W. Stefanowicz, B. Faina, T. Li, T.E. Winkler, D. Sztenkiel, A. Navarro-Quezada, M. Rovezzi, R. Jakiela, A. Grois, M. Wegscheider, W. Jantsch, J. Suffczynski, F. D'Acapito, A. Meingast, G. Kothleitner, T. Dietl, Phys. Rev. B 84 (2011) 035206.
[10] O. Sancho-Juan, O. Martinez-Criado, A. Cantarero, N. Garro, M. Salome, J. Susini, D. Olguin, S. Dhar, K. Ploog, Phys. Rev. B 83 (2011) 172103.
[11] W. Stefanowicz, D. Sztenkiel, B. Faina, A. Grois, M. Rovezzi, T. Devillers, F. d'Acapito, A. Navarro-Quezada, T. Li, R. Jakiela, M. Sawicki, T. Dietl, A. Bonanni, Phys. Rev. B 81 (2010) 235210.
[12] N. Smolentsev, G. Smolentsev, S. Wei, A.V. Soldatov, Phys. B 406 (2011) 2843.
[13] X. Biquard, O. Proux, J. Cibert, D. Ferrand, H. Mariette, R. Giraud, B. Barbara, J. Supercond. 16 (2003) 127.
[14] S. Kuroda, S. Marcet, E. Bellet-Amalric, J. Cibert, H. Mariette, S. Yamamoto, T. Sakai, T. Ohshima, H. Itoh, Phys. Status Solidi A-Appl. Mater. 203 (2006) 1724.
[15] A. Singh, R. Kumar, P. Thakur, N. Brookes, K. Chae, W. Choi, J. Phys.: Condens. Matter 21 (2009) 185005.
[16] J.A. Sans, G. Martinez-Criado, J. Susini, R. Sanz, J. Jensen, I. Minguez, M. Hernandez-Velez, A. Labrador, P. Carpentier, J. Appl. Phys. 107 (2010) 023507.
[17] J. Baik, S. Kim, Y. Koo, T. Kang, J. Lee, Electrochem. Solid State Lett. 7 (2004)

[18] C. Liu, E. Alves, A. Ramos, M. da Silva, J. Soares, T. Matsutani, M. Kiuchi, Nucl. Instr. Meth. Phys. Res. Sect. B 191 (2002) 544.
[19] L.M.C. Pereira, U. Wahl, J.G. Correia, S. Decoster, L.M. Amorim, M.R. da Silva, J.P. Araujo, A. Vantomme, Phys. Rev. B 86 (2012) 195202.
[20] L.M.C. Pereira, U. Wahl, S. Decoster, J.G. Correia, L.M. Amorim, M.R. da Silva, J.P. Araujo, A. Vantomme, Phys. Rev. B 84 (2011) 125204.
[21] U. Wahl, A. Vantomme, G. Langouche, J.G. Correia, L. Peralta, Appl. Phys. Lett. 78 (2001) 3217.
[22] E. Rita, U. Wahl, J. Correia, E. Alves, J. Soares, Appl. Phys. Lett. 85 (21) (2004) 4899.
[23] H. Hofsass, G. Lindner, Phys. Rep. 201 (3) (1991) 121.
[24] U. Wahl, J.G. Correia, S. Cardoso, J.G. Marques, A. Vantomme, G. Langouche, ISOLDE Collaboration, Nucl. Instr. Meth. Phys. Res. B 136 (1998) 744.
[25] S. Agostinelli et al., Nucl. Instr. Meth. Phys. Res. Sect. A 506 (2003) 250.
[26] J. Allison et al., IEEE Trans. Nucl. Sci. 53 (2006) 270.
[27] P. Boguslawski, E.L. Briggs, J. Bernholc, Phys. Rev. B 51 (1995) 17255.
[28] V.N. Fedoseyev, K. Batzner, R. Catherall, A.H.M. Evensen, D. ForkelWirth, O.C. Jonsson, E. Kugler, J. Lettry, V.I. Mishin, H.L. Ravn, G. Weyer, Nucl. Instr. Meth. Phys. Res. Sect. B 126 (1) (1997) 88.
[29] J.F. Ziegler, M.D. Ziegler, J.P. Biersack, Nucl. Instr. Meth. Phys. Res. Sect. B 268 (2010) 1818.
[30] U. Wahl, J.G. Correia, A. Czermak, S.G. Jahn, P. Jalocha, J.G. Marques, A. Rudge, F. Schopper, J.C. Soares, A. Vantomme, P. Weilhammer, ISOLDE Collaboration, Nucl. Instr. Meth. Phys. Res. Sect. A 524 (2004) 245.
[31] M.R. Silva, U. Wahl, J.G. Correia, L.M. Amorim, L.M.C. Pereira, Rev. Sci. Instrum. 84 (2013) 073506.
[32] U. Wahl, A. Vantomme, G. Langouche, J. Araujo, L. Peralta, J.G. Correia, ISOLDE Collaboration, J. Appl. Phys. 88 (2000) 1319.
[33] F. Takano, H. Ofuchi, J. Lee, K. Takita, H. Akinaga, Phys. B 376 (2006) 658.